Stabilization of Aqueous Carbon Nanotube Dispersions Using Surfactants: Insights from Molecular Dynamics Simulations

Naga Rajesh Tummala, Brian H. Morrow, Daniel E. Resasco, and Alberto Striolo*

School of Chemical, Biological, and Materials Engineering, The University of Oklahoma, Norman, Oklahoma 73019, United States

ABSTRACT Techniques for separating bundles of carbon nanotubes into homogeneous dispersion are still under development, although a few methods have been successful at the laboratory scale. Understanding the effective interactions between carbon nanotubes in the presence of dispersing agents will provide the necessary information to develop better methods and also to refine the existing ones. We present here results from all-atom molecular dynamics simulations for aqueous flavin mononucleotide (FMN), which has been found experimentally to efficiently separate single-walled carbon nanotubes (SWNTs) based on diameter and chirality. We report results for the aggregate morphology of FMN on SWNTs of different diameters, as well as the potential of mean force between (6,6) SWNTs in the presence of aqueous FMN. The results are compared to the potential of mean force between SWNTs in aqueous sodium dodecyl sulfate (SDS). Our detailed analysis is used to explain the role of FMN, water, and sodium ions in providing a strong repulsive barrier between approaching SWNTs.

KEYWORDS: flavin mononucleotide · sodium dodecyl sulfate · potential of mean force

Single-walled carbon nanotubes (SWNTs) are one-dimensional materials with exceptional mechanical,[1] electrical, thermal,[2] and electronic properties.[3] Application of single-walled carbon nanotubes in electronic[4] or opto-electronic[5] devices requires their efficient separation based on chirality and diameter. Their use in therapeutics[6,7] and composites[8] requires homogeneous dispersions within cellular environment or organic materials, respectively. Hence, separating and dispersing SWNTs continues to attract scientific attention. There has been success in separating SWNTs by density gradient centrifugation, especially at the laboratory scale, using a variety of surfactants.[3,9−16] Recently, DNA sequences that can selectively sort nanotubes based on chirality were discovered,[17] although their applicability to large-scale separations is not yet feasible. A simple gel-based method to separate metallic from semiconducting SWNTs, which appears to be easily scalable, has also been reported.[18,19] Several excellent reviews are available concerning the state of the art of separating SWNTs after production or of selectively growing SWNTs based on their chirality and diameter.[20−23]

Different surfactants yield a variety of molecular structures on SWNTs. These structures are thought to determine the buoyancy differences utilized in centrifugation-based separation methods. Scattering experiments[24] and molecular dynamics (MD) simulations can be used, complementarily, to investigate such structures.[25−31] It is known from experiments[24] and simulations[25−31] that sodium dodecyl sulfate (SDS) yields various disordered aggregates on SWNTs at different surface densities. At low surface density, aqueous SDS surfactants yield rings around SWNTs. Increasingly disordered aggregates form with increasing surface density.[24,28,29,32] Using coarse grained simulations, researchers have found that many different aggregate morphologies are possible on SWNTs.[32] MD simulations for the aggregate structure of a SWNT covered with SDS at high surfactant coverage[33] and the potential of mean force between SWNTs in the presence of SDS were recently reported.[33,34] The results show that the potential of mean force between the SWNTs is affected by the structure and morphology of the surfactant aggregates. Experimentally, it has been observed that excessive surfactant can result in flocculation of nanotubes,[35] and that surfactants at very low concentrations cannot efficiently disperse SWNTs.[3,9−11,13] For biological applications, the use of SDS, as well as that of sodium dodecyl benzene sulfonate (SDBS), may result in cytotoxicity.[36] Hence the use of biologically benign amphiphilic molecules like sodium cholate[16]

*Address correspondence to astriolo@ou.edu.

Received for review August 5, 2010 and accepted November 22, 2010.

Published online December 3, 2010.
10.1021/nn101929f

© 2010 American Chemical Society

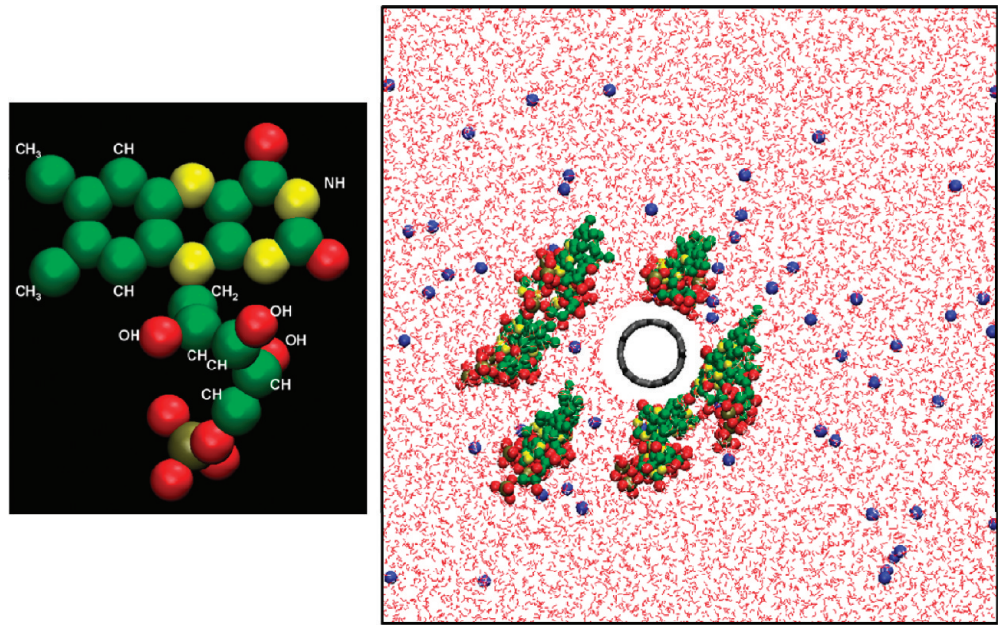

Figure 1. Left: FMN molecule. Green spheres represents aromatic carbon atoms, −CH, $-CH_2$, or $-CH_3$ groups; yellow spheres represent nitrogen and −NH; red spheres represent oxygen atoms in phosphate groups and isoalloxazine as well as −OH groups in the D-ribityl chain; tan spheres represent phosphorus atoms. Right: Initial configuration of FMN molecules around one (6,6) SWNT. The blue spheres represent sodium counterions. Water molecules, red, are represented in the wireframe convention. The gray circle corresponds to the (6,6) SWNT. All images were prepared using the VMD visualization suite.[37]

and flavin mononucleotide (FMN)[14,15] has gained prominence. The presence of planar aromatic cyclic structures in the surfactants is considered the main reason for the observed effectiveness in dispersing and separating SWNTs. To design nanotube-specific stabilization processes, it is necessary to determine the surfactant aggregate morphologies on SWNTs of various diameters. Comparing such results obtained for FMN to those available for SDS will allow us to better understand the effect of surfactant molecular structure on the effectiveness in dispersing SWNTs.

In this study, we report the aggregate morphologies of FMN on SWNTs with different diameters as obtained *via* all-atom MD simulations. Simulation details are reported in Appendix 2. A schematic of the simulated system is shown in Figure 1. We also compute the potential of mean force (PMF) between two (6,6) armchair SWNTs in aqueous FMN and SDS at two surface densities. We compare the PMFs obtained from our study to those available in the literature[33] to understand the effect of the amphiphilic surface density on the SWNT−SWNT PMF.

RESULTS

Aggregate Structure. In Figure 2, we show representative simulation snapshots of 29 FMN molecules adsorbed on (6,6), (8,6), (12,12), and (16,16) SWNTs. The available surface area per each FMN is ∼0.94, ∼1.03, ∼1.48, and ∼1.84 nm^2 on (6,6), (8,6), (12,12), and (16,16) SWNTs, respectively. Because FMN in the bulk can only self-aggregate forming dimers,[38] most of the FMN molecules simulated herein remain on the SWNT surface. In general, our results show that the FMN isoalloxazine group remains for the most part adsorbed on the SWNT walls, while the D-ribityl phosphate group extends toward the aqueous phase. On SWNTs of diameter <1.0 nm [(6,6) and (8,6) SWNTs], most of the SWNT surface is completely covered by FMN molecules. Additional FMN molecules agglomerate within the aqueous solution, while parts of the (12,12) and (16,16) SWNT surfaces are exposed to water when there are the same number of FMN molecules present on the SWNT surface. The formation of the helical 8_1 configuration, proposed[14,15,39] on (8,6) SWNT, requires a surface density of ∼0.75 nm^2 per FMN molecule. Even though we employed ∼1.03 nm^2 per FMN molecule on (8,6) SWNTs, we observe FMN molecules away from the SWNT surface (see Figure 2). This suggests that the formation of 8_1 helical assemblies is hindered, likely by large entropic barriers. It is possible that the process of ultracentrifugation, or very high bulk FMN concentrations, promotes the formation of the helical structure observed *via* energy minimization calculations.[14] It should be pointed out that in the simulations supporting the formation of 8_1 helical assemblies,[39] preformed structures were compared. In the simulation presented here, the FMN aggregates form spontaneously depending on the evolution of the system, which obey the equations of motion. Because of the careful methodology implemented, we are confident that the aggregate structures shown in Figure 2 correspond to equilibrium structures. However, as it is always the case in simulations, the results strongly depend on the force fields implemented. It is possible that the force fields implemented herein, al-

though widely used, are somewhat deficient to study the structure of FMN aggregate on nanotubes.

From Figure 2, it is also clear that sodium ions are strongly correlated to the phosphate groups, as expected because of electrostatic interactions. Although the effect of divalent counterions has not been explicitly considered herein, it is likely that, because of counterion−condensation phenomena, the morphology of the surfactant aggregates changes upon changes in salt concentration and salt type.

To study the differences between the orientations of FMN molecules on SWNTs of different diameters, we computed the angle between the vector formed by the two nitrogen atoms in the central ring of the isoalloxazine group (see Figure 1) and the SWNT axis (parallel to the *z*-axis of the simulation box). We also compute density distributions of isoalloxazine groups, D-ribityl phosphate groups, and sodium counterions away from the SWNT surface. We report these results in Figure 3.

The density distribution for isoalloxazine groups away from the SWNT surface is shown in the top left panel of Figure 3. We observe a strong peak at 4.0 Å, indicating that most of the FMN molecules are adsorbed on the nanotube surface with their isoalloxazine group lying on the carbon atoms. On (6,6) and (8,6) SWNTs, we observe small peaks at 8.0 and ~10.0 Å, corroborating the observation from the representative snapshots in Figure 2, according to which on these nanotubes a few FMN molecules remain away from the SWNT surface. The homogeneous density distribution of D-ribityl phosphate groups observed from ~3.0 to ~10.0 Å (top right panel of Figure 3) indicates that these groups extend away from the SWNT surface. The peaks observed on (12,12) and (16,16) SWNTs are less intense than those on (8,6) and (6,6) SWNTs because the FMN surface density is less on the former than on the latter tubes. The sodium counterions (bottom left panel of Figure 3) are strongly associated with the phosphate groups, as both density profiles show peaks located ~10.0 Å from the SWNT surface.

For the calculation of the orientation probabilities (bottom right panel of Figure 3), only those isoalloxazine groups that are closer than 5.5 Å from the SWNT surface are considered. An angle of 0° indicates that the long axis of the isoalloxazine group is perpendicular to the SWNT axis. An angle of 90° indicates that the long axis of the isoalloxazine group is parallel to the SWNT axis. On all of the nanotubes, we observe that the majority of the FMN isoalloxazine groups favor being parallel to the SWNT axis, which is consistent with the formation of 8_1 helical assembly.[14,39] However, even on (6,6) and (8,6) SWNTs, we find a few FMN molecules with the long axis of the isoalloxazine group perpendicular to the SWNT axis. Such orientation is not consistent with the formation of helical assemblies, and it is probably due to entropic effects. This result is consistent with data from tight-binding density functional methods, which show that the adsorption energy of flavin adenine dinucleotide (FAD) molecules is similar for both parallel and perpendicular orientation on semiconducting (10,0) and metallic (5,5) SWNTs.[40]

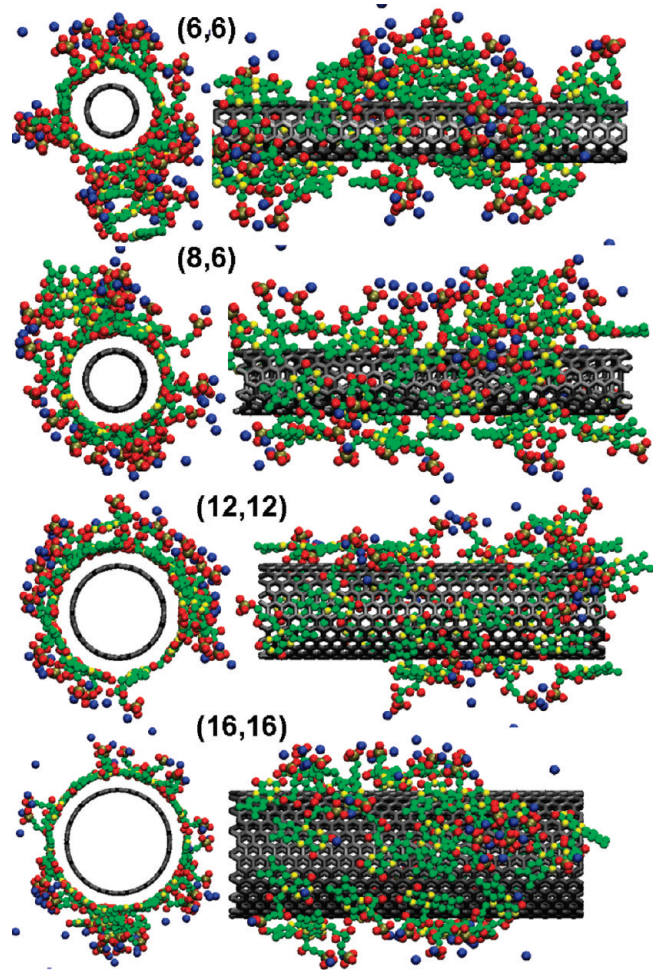

Figure 2. Front and side view of representative simulation snapshots for FMN molecules on SWNTs of different diameters. From top to bottom the results are for (6,6), (8,6), (12,12), and (16,16) SWNTs, respectively. The color code is the same as that in Figure 1. Water molecules are not shown for clarity.

We find very few molecules oriented at 0 or 180° on (12,12) SWNTs, whereas a few noticeable peaks in the orientation distribution corresponding to these angles can be observed on (16,16) SWNTs. These results indicate that the FMN molecules yield aggregates with somewhat different morphologies on SWNTs of different diameter, which may result in nanotube-specific properties that, for example, have been exploited experimentally for the purification of (8,6) SWNTs.[14] However, we point out that the differences observed on (6,6) or (8,6) SWNTs, which have similar diameter but different chirality, in terms of both density profiles and orientation of the adsorbed molecules are minimal. This is probably a consequence of the fact that in our simulations the electronic structure of the nanotubes (*e.g.*, metallic *vs* semiconducting) is not taken into consideration.

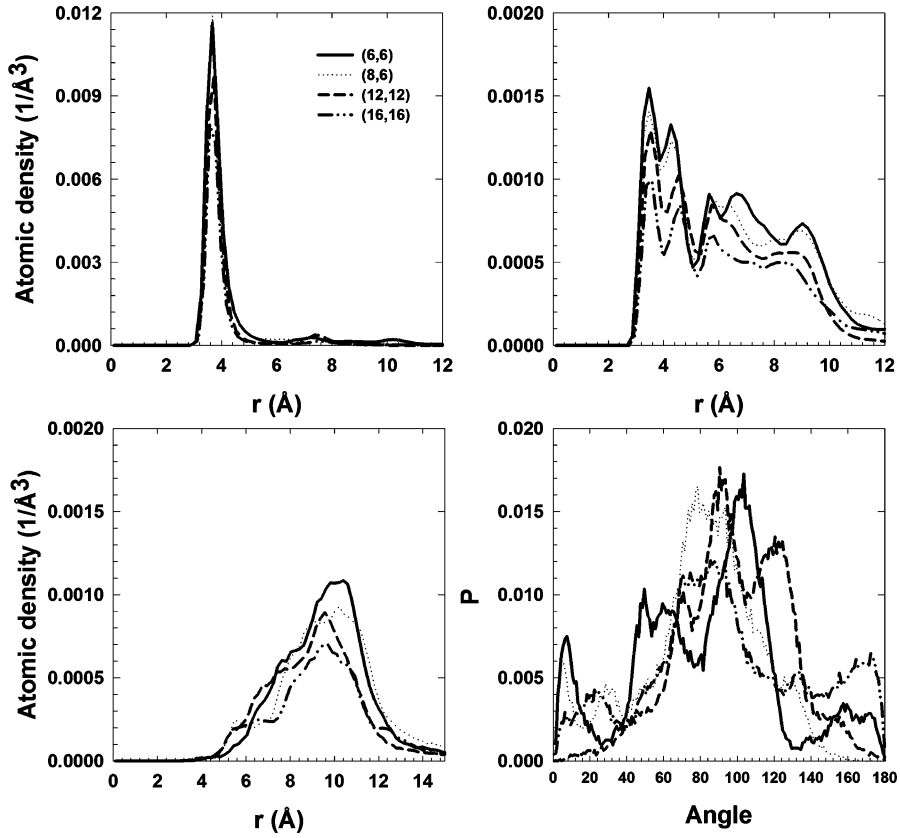

Figure 3. Density distribution of isoalloxazine groups of FMN (top left), D-ribityl phosphate groups of FMN (top right), and sodium counterions (bottom left). Orientation probability of isoalloxazine groups of FMN on SWNTs of different diameters (bottom right). Different lines are for results obtained on SWNTs of different diameters.

Potentials of Mean Force. Potential of mean force (PMF) calculations show how one SWNT interacts with another SWNT in the presence of water and adsorbed surface aggregates. A positive PMF indicates an effective repulsion; a negative PMF indicates effective attraction. Results for PMF between fullerenes and SWNTs in water have been reported.[41,42] Strong attraction at short separation (less than 5 Å) and water-induced repulsion due to hydrated layers at medium separations (~5−10 Å) are common features. The water-induced repulsion is, however, not strong enough to hinder the agglomeration of SWNTs in water. Of course, the strength of the effective interactions predicted by simulations varies with changes in the interaction parameters implemented. Despite these limitations, PMF calculations remain valuable in providing physical insights that could be used to design SWNT-specific dispersing agents.

The distance reported on the *x*-axis of Figure 4 is that between the SWNT surfaces, measured as the distance between the centers of the carbon atoms on the nanotubes surfaces. The corresponding SWNT−SWNT center-to-center distance is obtained by adding the diameter of the (6,6) SWNT (8.12 Å) to the distance reported on the *x*-axis. In Figure 4, we compare the PMF profiles of aqueous SWNTs in the presence of SDS at low and high surface coverage. The results are compared to those obtained in water. The PMF is set to zero at large separations between the SWNTs.

For rigid SWNTs in water, we observe strong water-induced repulsion peaks at ~5.0, ~8.0, and ~12.0 Å, corresponding to one, two, and three hydration layers. The rigidity of the tube allows for strongly hydrogen bonded water layers, and hence, the magnitude of the PMFs' repulsion and attraction are far higher in the case of rigid SWNTs than it is for flexible SWNTs (results obtained for flexible SWNTs, not reported here for brevity, show less pronounced PMF peaks). We found more wa-

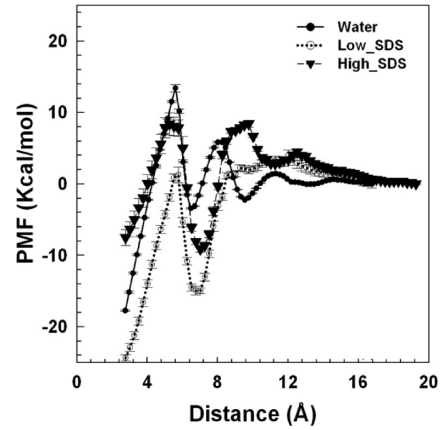

Figure 4. Potential of mean force between two rigid (6,6) SWNTs in water and in aqueous SDS.

ter molecules between two rigid tubes than between two flexible nanotubes (not shown), especially when the distance between the SWNT surfaces is 4−6 Å.

For PMFs between SWNTs in aqueous SDS, at ~10.0 Å we observe a rather strong repulsive barrier between SWNTs covered with SDS at high surface coverage (~10.0 kcal/mol). The repulsive peak is much weaker at low SDS surface densities (~3−4 kcal/mol). At both coverages, an attractive region is observed at ~11.0 Å, followed by a repulsion at ~13.0 Å and a small inflection in the PMF profile at ~16.0 Å (especially in the case of high surface coverage). The PMF profile between SWNTs at high SDS coverage is zero at separations larger than 18.0 Å. Recent results, obtained at much higher surface density than those considered herein, have reported the maximum in the repulsion between SWNTs at ~16.0 Å.[33] The PMF at d ~ 3.0 Å (corresponding to SWNTs at contact with each other) is negative, indicating that it is thermodynamically not possible to promote the dispersion of individual (6,6) SWNTs in aqueous systems using SDS at the conditions considered here.

All simulations indicate that the SWNT−SWNT PMF becomes repulsive when the SDS aggregates, adsorbed on the nanotubes, overlap. Consequently, the PMF repulsive peak appears at ~10.0 Å and no strong SWNT−SWNT PMF is observed at distances greater than ~10.0 Å. At low SDS coverage, a monolayer forms in which SDS molecules orient parallel to the tube surface.[28,29] Our results indicate that SDS molecules at low coverage on SWNTs are very mobile. At short SWNT−SWNT distance, they tend to accumulate between the interacting tubes because in so doing one SDS molecule interacts with both SWNT surfaces simultaneously. Unfortunately, when this happens, a portion of the SWNT surface remains exposed to water, which may lead to nanotube aggregation. A snapshot is provided in Figure 5 to illustrate this situation.

When the SDS surface density is increased, the SDS molecules between approaching SWNTs provide a stronger repulsion (~10.0 kcal/mol) because more work is required to disperse the SDS molecules aggregated on the SWNT surface. At even higher surface density, Xu *et al.* reported a repulsive barrier at ~16.0 Å of much greater magnitude than those observed in our simulations.[33] We observe strong attraction at ~7−8 Å (as the two surfactant layers between SWNTs give way to only one surfactant layer). Similar oscillatory forces are often observed when solvent molecules form layers between two approaching surfaces.[43−46] As a consequence of such effects, we observe a strong attractive peak located at ~7.0−8.0 Å, in agreement with DFT calculations by Patel and Egorov.[47] Even the results obtained by Xu *et al.* predict attraction at ~7.0 to 8.0 Å.[33] It is worth pointing out that the strongest attractive PMF between (6,6) SWNTs is observed at ~7.0−8.0 Å at high SDS coverage and at ~3.0 Å at low SDS coverage. This

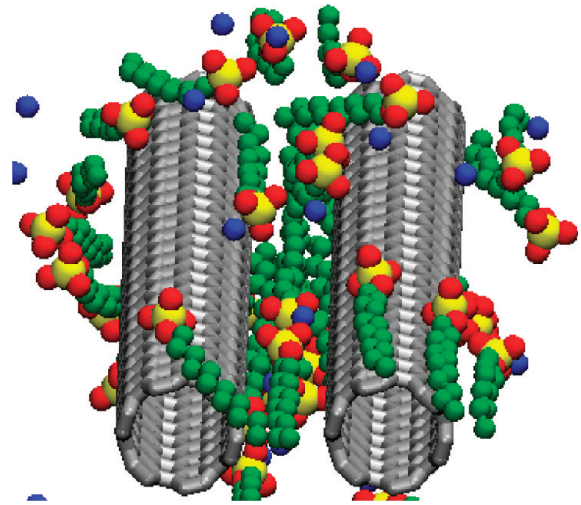

Figure 5. Representative simulation snapshots for SDS aggregates on two approaching SWNTs at low SDS surface coverage. The SWNTs are separated by 6.90 Å. Green, red, and yellow spheres represent methyl groups, oxygen, and sulfur atoms of SDS, respectively. Blue spheres represent sodium ions. Carbon atoms in nanotubes are connected with bold gray lines. Water is not shown for clarity.

suggests that a complex formed by two SWNTs and one layer of SDS surfactants between can be more stable than SWNT bundles in the presence of SDS at high surface densities. This observation appears to be consistent, to some extent, with the experimental observation according to which SDS at high surface densities can keep SWNTs dispersed for some time.[3,9,10]

The PMFs between SWNTs at low and high FMN surface coverage are shown in Figure 6, where the results are also compared to those obtained in water and aqueous SDS. It is evident from Figure 6 that adsorbed FMN molecules provide intense long-range stepwise repulsive barriers which become stronger as the distance decreases. Each step observed in the PMF corresponds to a reorganization of FMN molecules in the volume between the two approaching SWNTs, as discussed below.

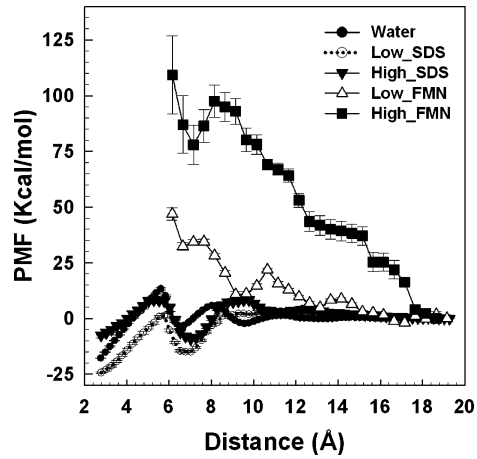

Figure 6. Potential of mean force between two rigid (6,6) SWNTs in water, in aqueous SDS, and in aqueous FMN. For both surfactants, results are reported at two surface coverages [low (0.98 nm^2/SDS and 1.24 nm^2/FMN) and high (0.44 nm^2/SDS and 0.94 nm^2/FMN)].

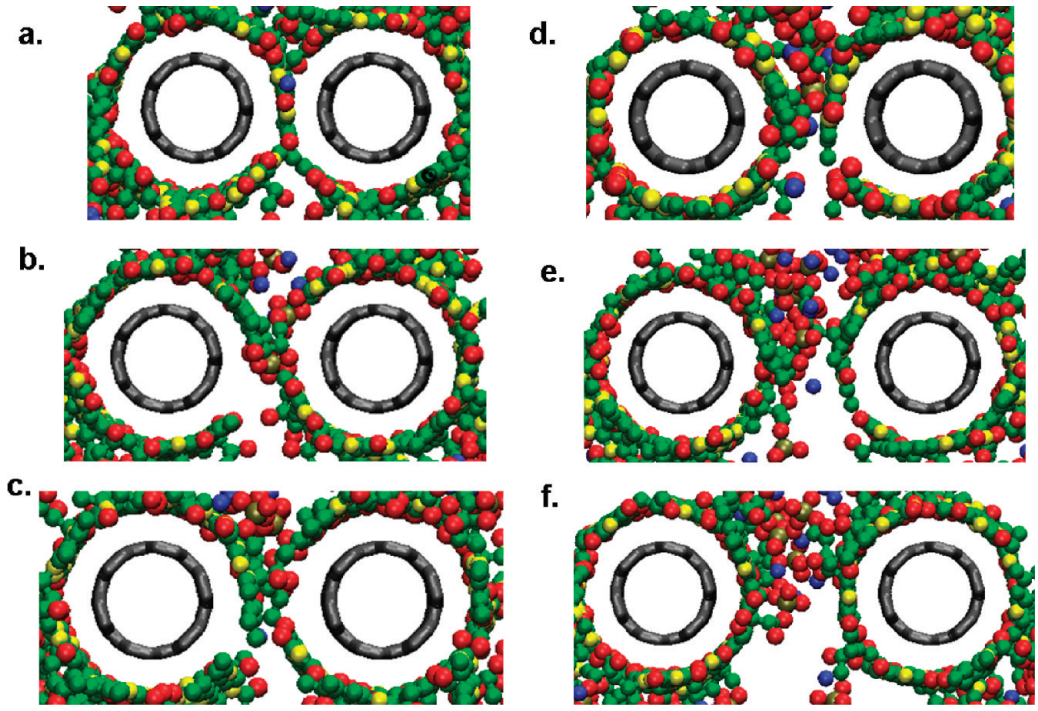

Figure 7. Representative simulation snapshots for FMN aggregates on approaching SWNTs at low FMN surface coverage. Results are shown at various SWNT−SWNT separations, corresponding to steps in the PMF profile. SWNTs are separated by (a) 6.15 Å, (b) 8.90 Å, (c) 9.15 Å, (d) 10.90 Å, (e) 13.65 Å, and (f) 14.90 Å. The color code is the same as that in Figure 1. Water is not shown for clarity.

We could not sample the configurations corresponding to distances shorter than ~6.0 Å between SWNTs, as the expulsion of the last FMN molecule from the volume between the approaching SWNTs is statistically prohibitive. Hence, the PMF profiles between SWNTs in presence of FMN are not computed for distances less than ~6.0 Å. Because we do not have data for the PMF at contact between the (6,6) SWNTs, we cannot comment on the thermodynamic stability of aqueous dispersions of (6,6) SWNTs in the presence of FMN, although the results in Figure 6 suggest that individually dispersed nanotubes may be thermodynamically stable. Certainly, the PMFs reported in Figure 6 in the presence of FMN are consistent with a substantial kinetic barrier that should prevent dispersed (6,6) SWNTs from aggregating.

We discuss the rearrangement of FMN aggregates in conjunction with details of the PMF profile only at low FMN surface coverage since the changes in aggregate morphology with distance are more evident at such conditions. Representative simulation snapshots of FMN molecules assembled around the approaching SWNTs are shown in Figure 7. When the distance between the SWNT surfaces is greater than twice the extended length of the FMN D-ribityl phosphate groups, the SWNT−SWNT PMF oscillates around zero.

Noticeable steps in the PMF profile occur at ~15.0, ~13.0, ~11.0, ~9.0, ~8.0, and ~6.0 Å. Decreasing the distance between the SWNTs to ~18.0 Å, we notice that the phosphate groups and counterions from each of the two interacting FMN−SWNT aggregates begin to overlap, causing the first repulsive step. The repulsive interaction increases until the phosphate groups of FMN on one of the two SWNTs are expelled out of the intertube region, as observed in panel f of Figure 7 (d = ~14.0 Å). The phosphate groups continue to move out of the region between the interacting SWNTs as the distance decreases. The next step in the PMF profile occurs at ~13 Å, at which distance we observe phosphate groups of FMN on only one SWNT between the SWNTs (panel e in Figure 7). Decreasing further the SWNTs separation reduces the volume between the tubes, and the D-ribityl phosphate groups adsorbed on both the SWNTs are expelled from the region (panel d in Figure 7, d = ~11.0 Å), with related increase in steric repulsion. As the distance decreases further, the D-ribityl phosphate groups are expelled from the region between the SWNTs and the solvent enters into the intertube space. The PMF becomes less repulsive from ~11.0 to ~9.0 Å (see Figure 6), indicating that the expulsion of water molecules between the FMN−SWNT aggregates is energetically favorable. A representative snapshot of the FMN−SWNT aggregate at 9.15 Å separation between SWNTs is shown in panel c of Figure 7. In this snapshot, we observe a few isoalloxazine groups adsorbed on the two approaching SWNTs. Decreasing the distance between the SWNTs further involves expelling the last strongly adsorbed FMN molecules from the region between the SWNTs. This process involves a strong energetic penalty and yields a stepwise increase in the PMF profile from ~9.0 to 6.0 Å. When the distance between the SWNTs is just greater than the dis-

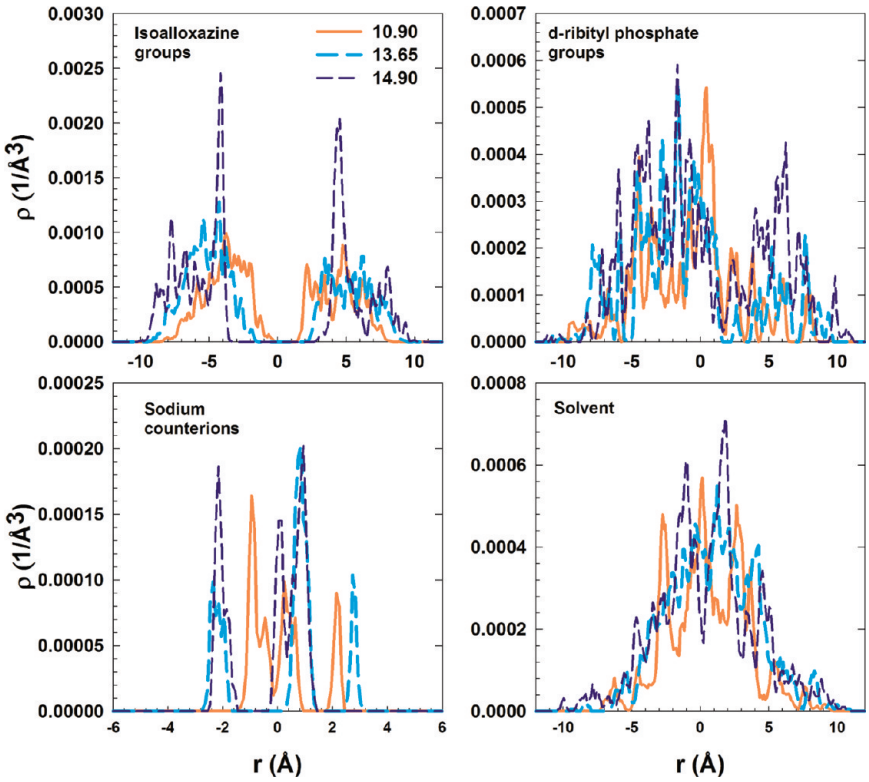

Figure 8. Density distribution of isoalloxazine groups (top left) and D-ribityl groups (top right) of FMN molecules, sodium counterions (bottom left), and water (bottom right) at 10.90 Å (continuous line), 13.65 Å (thick dashed line), and 14.90 Å (thin dashed line) intertube separation between two (6,6) SWNTs at low FMN surface coverage.

tance required to fit one layer of isoalloxazine groups between the SWNTs, we observe a plateau in the PMF profile. When the separation between SWNTs equals the sum of the excluded radii of SWNTs and isoalloxazine group (~6.0 Å, the snapshot shown in panel a of Figure 7 corresponds to 6.15 Å), we observe a strong repulsion.

To further quantify the phenomena discussed in Figure 7, we study the density of various components around and between the approaching SWNTs. The density distribution of FMN moieties, sodium ions, and water molecules within a rectangular box connecting the centers of mass of the two interacting SWNTs and extending over the diameter of the SWNT and their excluded radii are shown in Figure 8 and Figure 9. The two figures contain results at the various distances used in Figure 7. Although the density distributions of D-ribityl phosphate groups do not convey any important information, we present them for completeness. Decreasing the distance between SWNTs from 14.90 to 13.65 Å, we observe that the density of isoalloxazine groups between the nanotubes decreases (top left panel of Figure 8). The density of atoms in D-ribityl phosphate group is 5 times less than that observed for the atoms of the isoalloxazine group. This indicates there are not many D-ribityl phosphate groups between the SWNTs at distances below 15.0 Å. The peaks in the density distribution of isoalloxazine groups (top left panel of Figure 8) correspond to the FMN molecules adsorbed on the SWNT surface along the line connecting the centers of mass of interacting SWNTs. At 10.90 Å, we observe a peak ~2.5 Å away from each SWNT, indicating that the FMN molecules on the SWNTs are compressed. In correspondence, a repulsion is observed in the PMF. The repulsion decreases as we further decrease the distance between the SWNTs. In most cases, the number of the peaks in the density profiles for sodium ions corresponds to the number of density peaks in density profile for water molecules (bottom panels of Figure 8), providing evidence of water−ion correlations.[48]

The density profiles for FMN, sodium, and solvent molecules at 9.15, 8.90, and 6.15 Å are shown in Figure 9. We observe that at 9.15 and 8.90 Å between nanotubes the density profile of water molecules in the volume between the nanotubes is almost identical. However, the density profile of sodium shows a single peak at 9.15 Å and multiple peaks at 8.90 Å; correspondingly, we observe an increase in the repulsion in the PMF profile at those distances. For the density distribution of isoalloxazine groups, we observe a transition from multiple peaks at 9.15 and 8.90 Å SWNT−SWNT separations to a single peak at 6.15 Å, confirming the expulsion of isoalloxazine groups from the volume between the nanotubes in correspondence to the strongest repulsion observed in the PMF profile.

The density distributions shown in Figure 8 and in Figure 9 could be used to predict the effective interaction between SWNTs through classical density func-

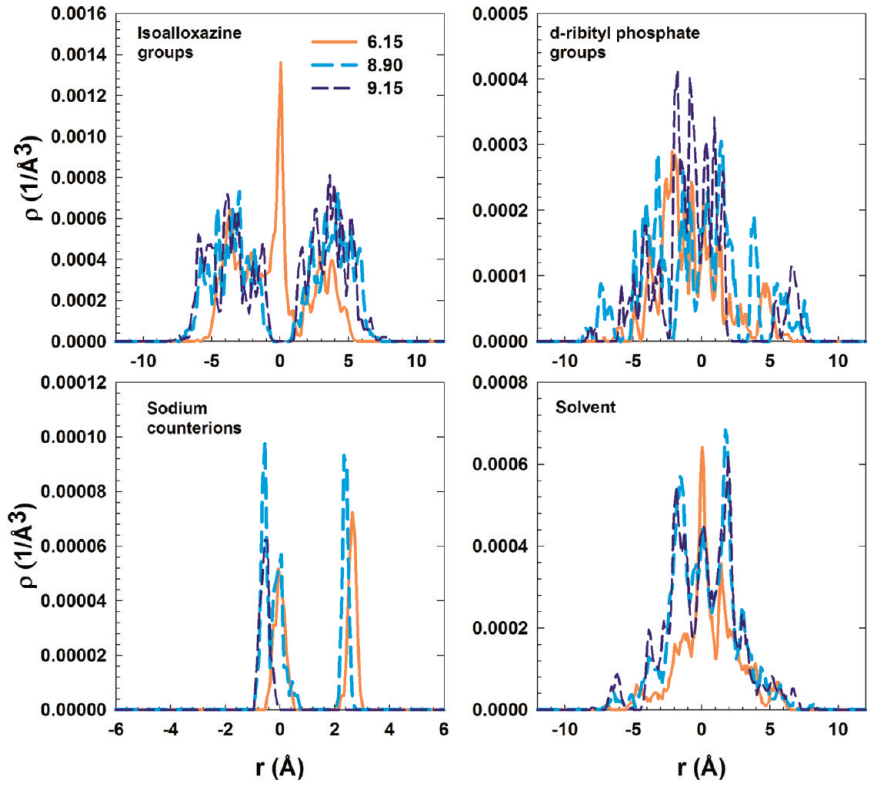

Figure 9. Same as Figure 8, but at distances of 6.15 Å (continuous line), 8.90 Å (thick dashed line), and 9.15 Å (thin dashed line).

tional methods, such as those reported by Patel and Egorov.[47] Detailed analysis for the structure of FMN surfactants, water molecules, and electrolytes as a function of the separation between the interacting carbon nanotubes at high FMN coverages is reported in Appendix 1.

CONCLUSIONS

All-atom molecular dynamics simulations were conducted for elucidating the morphology of aqueous FMN surfactants on single-walled carbon nanotubes (SWNTs) of various diameters. FMN molecules adsorb with the isoalloxazine group on the SWNT surface, yielding helical structures that resemble, to some extent, those proposed based on energy minimization techniques. However, the structures observed in our simulations are less compact than those proposed in the literature. We found that changing the SWNT diameter affects the orientation of FMN molecules and hence may enhance the separation of SWNTs based on diameter. Probably because our simulations do not account for changes in the electronic structure of SWNTs, we however do not observe significant changes in the surfactant aggregates when SWNT chirality changes at constant diameter.

We then calculated the effective pair potential of mean force (PMF) between aqueous (6,6) SWNTs in the presence of FMN at two surface densities. Increasing the surface density of FMN molecules increases the repulsive barrier between SWNTs. These results were compared to PMF data obtained between aqueous (6,6) SWNTs in the presence of SDS surfactants. On the basis of the PMF profiles, our results confirm experimental observations according to which FMN surfactants are far superior to SDS in stabilizing aqueous dispersions of SWNTs. To explain the physical mechanisms responsible for our observations, we calculated the density of FMN molecules, water, and counterions in the region between the interacting SWNTs at various nanotube−nanotube separations.

Although our simulations are dependent on the reliability of the force field implemented, they clearly suggest that to stabilize carbon nanotubes in water it is necessary to employ dispersing agents that (1) strongly adsorb on the nanotube surface, (2) present hydrophilic groups, better if rigid, that extend toward the aqueous phase, (3) are not very mobile on the nanotube surface, and (4) show aggregates with structure dependent on nanotube diameter and chirality. These observations could lead to the design of carbon-nanotube-specific dispersive agents.

Acknowledgment. The authors acknowledge financial support from the Carbon Nanotube Technology Center (CANTEC) at the University of Oklahoma, funded by the US DOE under contract DE-FG02-06ER64239, and from the National Science Foundation under contract CBET-0853759. Generous allocations of computing time were provided by the OU Supercomputing Center for Education and Research (OSCER) at the University of Oklahoma and by the National Energy Research Scientific Computing Center (NERSC) at Lawrence Berkeley National Laboratory.

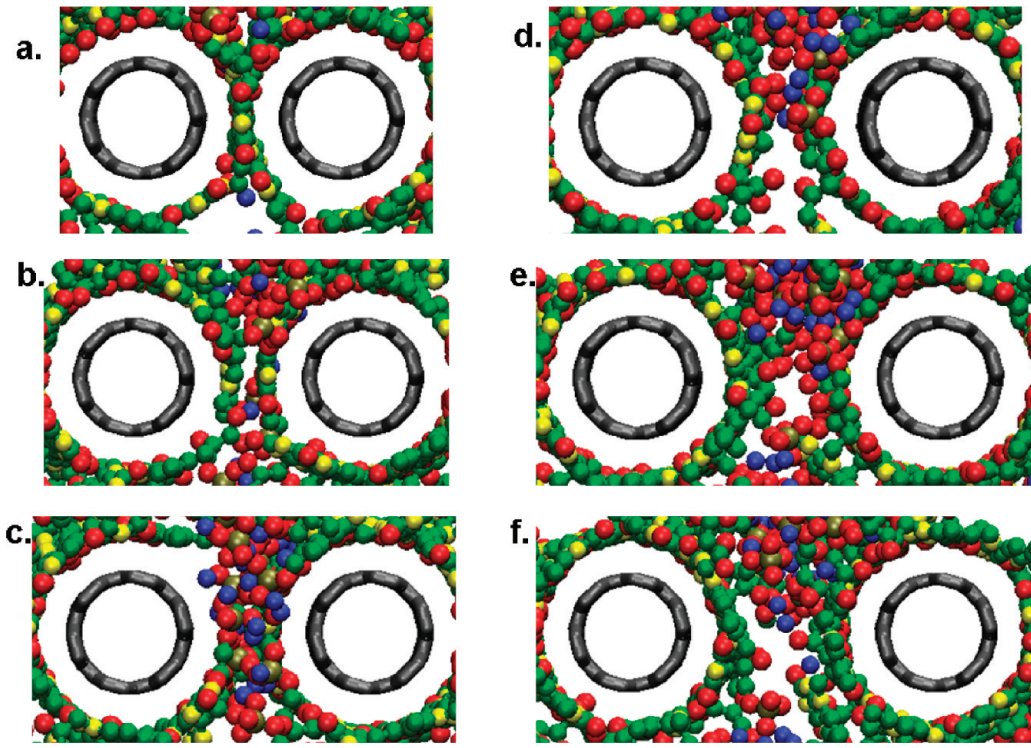

Figure 10. Representative simulation snapshots for FMN aggregates on approaching SWNTs at high FMN surface coverage. Results are shown at various SWNT−SWNT separations, corresponding to steps in the PMF profile. SWNTs are separated by (a) 6.15 Å, (b) 8.90 Å, (c) 9.15 Å, (d) 11.40 Å, (e) 13.65 Å, and (f) 14.90 Å. The color code is the same as that in Figure 1. Water is not shown for clarity.

APPENDIX 1: INTERACTING SWNTS IN THE PRESENCE OF FMN AT HIGH COVERAGE

The SWNT−SWNT PMF computed in aqueous FMN at high surface coverage shows about twice the repulsive barrier between SWNTs as compared to data at low surface coverage. The complete coverage of the SWNT surface with FMN molecules and the presence of few FMN molecules in the surrounding water cause the enhanced repulsive barrier. The PMF profiles show a stepwise profile similar to that observed at low FMN coverage. At high FMN coverage, the PMF profile either increases or remains constant at all distances, with the only exception observed at ~7.0−8.0 Å where the PMF decreases slightly. At similar separations, we found a plateau in the PMF profile at low FMN coverage. At high FMN coverage, decreasing the distance between SWNTs from ~9.0 to 7.0 Å significantly decreases the number of FMN molecules at contact with the SWNT surface. When this occurs, water molecules cannot enter the region between the nanotubes due to the high density of FMN molecules. The combination of these two phenomena leads to a reduced repulsion between nanotubes, which appears to be due to depletion effects.

For interacting SWNTs at large FMN surface density, we report simulation snapshots (Figure 10) and density distributions (Figure 11 and Figure 12) at various SWNT−SWNT distances. The molecular mechanisms responsible for the stepwise repulsive PMF shown in Figure 6 for high FMN coverage are analogous to those discussed at low FMN coverage. The only exception is that the effect of sodium counterions can be observed clearly at high FMN surface coverage. In the bottom left panel of Figure 12, we observe that the density of counterions decreases dramatically as the distance between SWNTs decreases from 9.15 to 8.90 Å. In correspondence, the PMF data show an increase in repulsive barrier in the PMF profile, suggesting that it is energetically not favorable to expel sodium ions from the region between the interacting SWNTs.

APPENDIX 2: SIMULATION METHODOLOGY

The extended simple point charge (SPC/E) model[49] was used to describe water molecules in our MD simulations. Recent work[50] suggests that polarizability effects are not significant in monovalent salt solutions since the field associated with monovalent ions does not significantly affect the water molecules within the hydration shell. The aggregate morphology of FMN was studied on (6,6), (8,6), (12,12), and (16,16) SWNTs, which are effectively considered infinitely long due to the implemented periodic boundary conditions. Although in our simulations the inside of the nanotubes is not accessible to solvent, ions, or surfactants, it should be noted that the presence of surfactants and water within the nanotubes[51] might affect their interactions and buoyancy. The center-to-center carbon−carbon distance across the nanotube diameter is 8.12, 9.46, 16.27, and 21.70 Å for the four nanotubes considered herein. SWNTs were maintained rigid during the course of the simulation. The force field parameters used for carbon atoms in the SWNT are identical to those used in our previous publications.[28,29] FMN molecules contain a tricyclic heteronuclear organic ring (isoalloxazine) and a D-ribityl phosphate group with affinity for polar solvents. FMN was modeled according to the AMBER force field.[52] In our model, the two −OH groups bonded to the phosphorus atom in the D-ribityl phosphate group are dissociated.[53] We substituted each hydrogen atom of those −OH groups with sodium counterions. The force field parameters used for sodium ions have been reported previously, together with the models implemented to simulate SDS.[54]

The leapfrog integration scheme within the GROMACS molecular dynamics simulation package[55−58] with a time step of 2 fs was used to integrate the equations of motion. A Berendsen barostat[59] with a time constant of 500 fs, compressibility of 4.5e-5 (1/bar), and reference pressure of 1 bar was used whenever the isobaric−isothermal ensemble (constant number of particles N, constant pressure P, and constant temperature T) was implemented. The canonical ensemble (constant number of particles N, volume V, and temperature T) was employed during the production phase. The Nosè−Hoover thermostat[60,61] with a time constant of 100 fs was used to maintain constant T. The particle mesh Ewald method[62] with cutoff of 1.4 nm and Fourier grid spaced with 0.12 nm, tolerance of 1×10^{-5}, and fourth order interpolation was used to compute the long-range electrostatic interactions. A switch function starting at 1.2 nm was used such that the Lennard-Jones potential smoothly goes to zero at 1.4 nm. During the production phase, one simulation

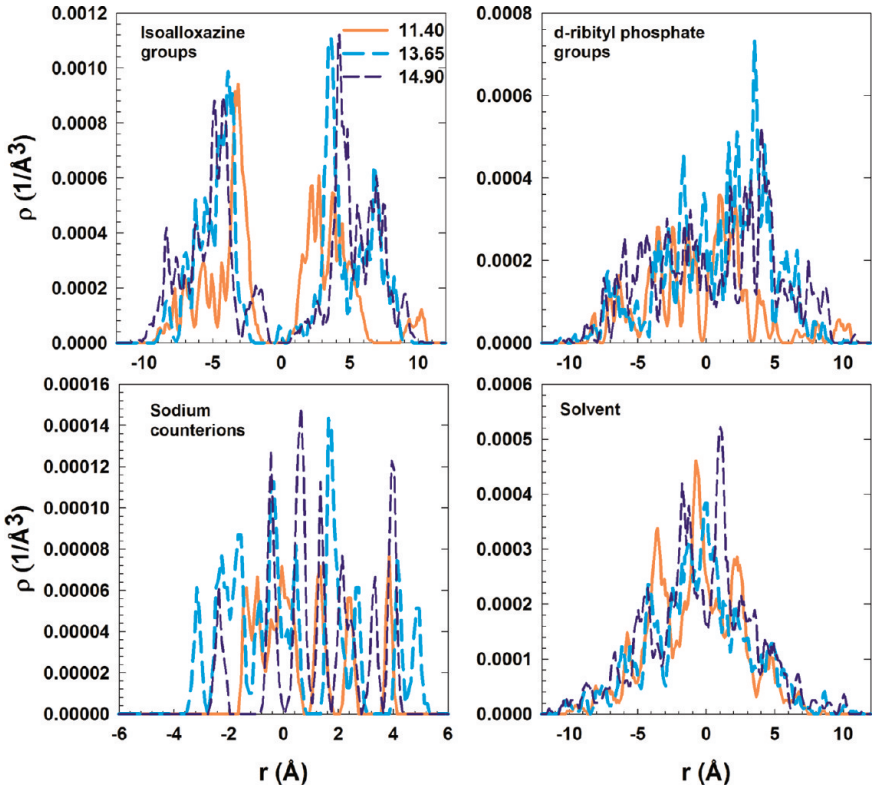

Figure 11. Density distribution of isoalloxazine groups (top left) and D-ribityl groups (top right) of FMN molecules, sodium counterions (bottom left), and water (bottom right) at 11.40 Å (continuous line), 13.65 Å (thick dashed line), and 14.90 Å (thin dashed line) intertube separation between two (6,6) SWNTs at high FMN surface coverage.

configuration was saved every 2 ps for analysis of the aggregate morphology.

Twenty-nine FMN molecules were concentrically placed around one SWNT as shown in Figure 1. Fifty-eight sodium ions, necessary to neutralize the 29 FMN molecules, were placed randomly throughout the simulation box. Water molecules were then used to fill the simulation box of size 8.0 × 8.0 × 6.15 nm^3. The NPT ensemble (P = 1 bar, T = 300 K) was used during the ini-

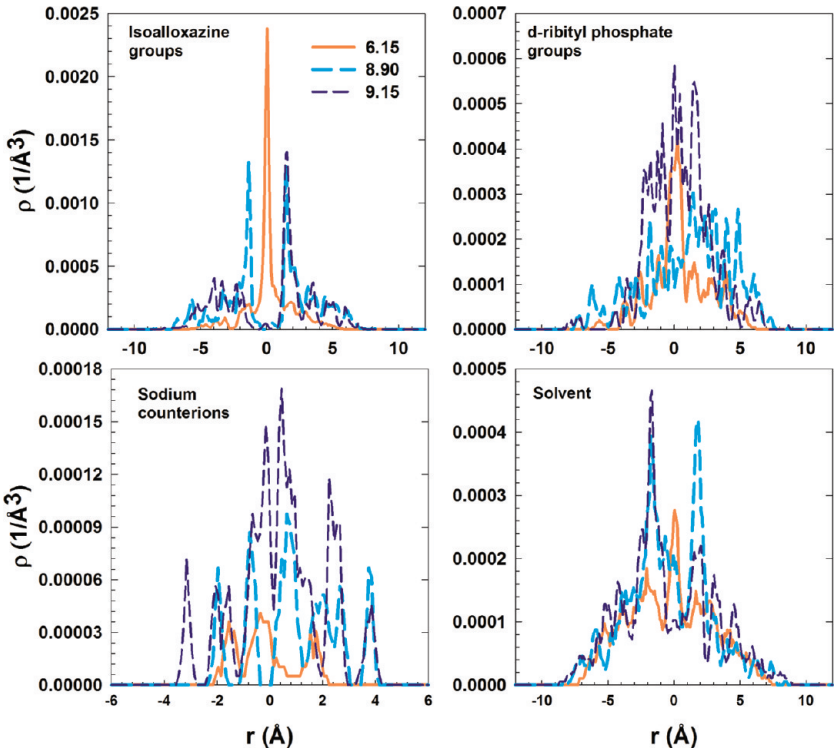

Figure 12. Same as Figure 11, but at separations of 6.15 Å (continuous line), 8.90 Å (thick dashed line), and 9.15 Å (thin dashed line).

tial equilibration phase to bring the system at ambient conditions. This phase lasted generally less than 5 ns. We conducted 30.0 ns of simulation in the NVT ensemble at 300 K, followed by 10.0 ns at 400 K, 10.0 ns at 500 K, and 20.0 ns at 300 K in the NVT ensemble. To ensure that the system was properly equilibrated, all groups bearing point charges in the FMN molecules were made neutral and the simulation was run for 20.0 ns in the NVT ensemble. This step was followed by reinsertion of charges and 30.0 ns of simulation in the NVT ensemble at 300 K. Thus each system was simulated for up to 120.0 ns. We compared the results computed from trajectories from 60.0 to 70.0 ns to those obtained from 100.0 to 110.0 ns. In all cases considered here, we did not observe any significant difference in the aggregate morphology of FMN molecules before removing the charges and after reinserting the charges on all the FMN groups.

We used the final equilibrium configuration of FMN on (6,6) SWNT and removed 7 FMN molecules and 14 sodium atoms to obtain a system with low FMN surface coverage. The surface area available for FMN is ~0.94 and ~1.24 nm^2 for high and low surface coverage, respectively.

We used both the high and low surface coverage on (6,6) SWNT to study the potential of mean force (PMF) between two (6,6) SWNTs. The equilibrium configuration of the FMN−SWNT system was replicated. The replicated FMN−SWNT aggregate was inserted parallel to the original one in a simulation box of size 7.75 × 7.22 × 6.1487 nm^3. Water molecules and sodium counterions were randomly placed throughout the box. The NPT ensemble was used to ensure that the system was simulated at ambient conditions. The simulation box was equilibrated for 20.0 ns. The final configuration was used as the starting configuration for 57 consecutive simulations, each conducted at a different separation between the SWNT centers of mass. The SWNTs were connected through a harmonic potential, following the umbrella sampling technique.[63−65] The SWNT−SWNT surface separation distances employed ranged from 3.0 to 15.0 Å. The force constant used for the harmonic potential ranged from 5 to 100 kcal/mol nm^2. We used 4.0 ns of equilibration at each separation followed by at least 3.0 ns of production phase in which the distance between the SWNTs' centers of mass were recorded every 20 fs. We employed the weighted histogram analysis method (WHAM)[66−68] to extract PMF profiles from the simulation trajectories.

Armchair (6,6) SWNTs were modeled as rigid cylinders, composed of discrete carbon atoms, which can translate only along the x-direction (perpendicular to the SWNTs axis).

For SDS on SWNTs, the two equilibrium configurations reported in our previous publication[28] with coverages corresponding to 0.98 and 0.44 nm^2 were used as starting configurations for PMF calculations. The PMFs were computed following the procedure described above, but within a simulation box of 8.5 × 7.57 × 6.15 nm^3, 5.0 ns equilibrium, and 5.0 ns production phase.

REFERENCES AND NOTES

1. Huang, J. Y.; Chen, S.; Wang, Z. Q.; Kempa, K.; Wang, Y. M.; Jo, S. H.; Chen, G.; Dresselhaus, M. S.; Ren, Z. F. Superplastic Carbon Nanotubes. *Nature* **2006**, *439*, 281.
2. Peters, J. E.; Papavassiliou, D. V.; Grady, B. P. Unique Thermal Conductivity Behavior of Single-Walled Carbon Nanotube−Polystyrene Composites. *Macromolecules* **2008**, *41*, 7274–7277.
3. O'Connell, M. J.; Bachilo, S. M.; Huffman, C. B.; Moore, V. C.; Strano, M. S.; Haroz, E. H.; Rialon, K. L.; Bout, P. J.; Noon, W. H.; Kittrell, C.; Jianpeng, M.; Hauge, R. H.; Weisma, R. B.; Smalley, R. E. Band Gap Flourescence from Individual Single-Walled Carbon Nanotubes. *Science* **2002**, *297*, 593.
4. Avouris, P.; Chen, Z.; Perebeinos, V. Carbon-Based Electronics. *Nat Nano* **2007**, *2*, 605–615.
5. Avouris, P.; Freitag, M.; Perebeinos, V. Carbon-Nanotube Photonics and Optoelectronics. *Nat. Photonics* **2008**, *2*, 341–350.
6. Mutlu, G. K. M.; Budinger, G. R. S.; Green, A. A.; Urich, D.; Soberanes, S.; Chiarella, S. E.; Alheid, G. F.; McCrimmon, D. R.; Szleifer, I.; Hersam, M. C. Biocompatible Nanoscale Dispersion of Single-Walled Carbon Nanotubes Minimizes *In Vivo* Pulmonary Toxicity. *Nano Lett.* **2010**, *10*, 1664–1670.
7. Kostarelos, K.; Bianco, A.; Prato, M. Promises, Facts and Challenges for Carbon Nanotubes in Imaging and Therapeutics. *Nat. Nanotechnol.* **2009**, *4*, 627–633.
8. Calvert, P. Nanotube Composites: A Recipe for Strength. *Nature* **1999**, *399*, 210–211.
9. Niyogi, S.; Boukhalfa, S.; Chikkannanavar, S. B.; McDonald, T. J.; Heben, M. J.; Doorn, S. K. Selective Aggregation of Single-Walled Carbon Nanotubes *via* Salt Addition. *J. Am. Chem. Soc.* **2007**, *129*, 1898–1899.
10. Niyogi, S.; Densmore, C. G.; Doorn, S. K. Electrolyte Tuning of Surfactant Interfacial Behavior for Enhanced Density-Based Separations of Single-Walled Carbon Nanotubes. *J. Am. Chem. Soc.* **2009**, *131*, 1144–1153.
11. Nair, N.; Kim, W. J.; Braatz, R. D.; Strano, M. S. Dynamics of Surfactant-Suspended Single-Walled Carbon Nanotubes in a Centrifugal Field. *Langmuir* **2008**, *24*, 1790–1795.
12. Strano, M. S.; Moore, V. C.; Miller, M. K.; Allen, M. J.; Haroz, E. H.; Kittrell, C.; Hauge, R. H.; Smalley, R. E. The Role of Surfactant Adsorption during Ultrasonication in the Dispersion of Single-Walled Carbon Nanotubes. *J. Nanosci. Nanotechnol.* **2003**, *3*, 81–86.
13. Matarredona, O.; Rhoads, H.; Li, Z.; Harwell, J. H.; Balzano, L.; Resasco, D. E. Dispersion of Single-Walled Carbon Nanotubes in Aqueous Solutions of the Anionic Surfactant NaDDBS. *J. Phys. Chem. B* **2003**, *107*, 13357–13367.
14. Ju, S.-Y.; Doll, J.; Sharma, I.; Papadimitrakopoulos, F. Selection of Carbon Nanotubes with Specific Chiralities Using Helical Assemblies of Flavin Mononucleotide. *Nat. Nanotechnol.* **2008**, *3*, 356–362.
15. Ju, S.-Y.; Kopcha, W. P.; Papadimitrakopoulos, F. Brightly Fluorescent Single-Walled Carbon Nanotubes *via* an Oxygen-Excluding Surfactant Organization. *Science* **2009**, *323*, 1319–1323.
16. Arnold, M. S.; Green, A. A.; Hulvat, J. F.; Stupp, S. I.; Hersam, M. C. Sorting Carbon Nanotubes by Electronic Structure Using Density Differentiation. *Nat. Nanotechnol.* **2006**, *1*, 60–65.
17. Tu, X.; Manohar, S.; Jagota, A.; Zheng, M. DNA Sequence Motifs for Structure-Specific Recognition and Separation of Carbon Nanotubes. *Nature* **2009**, *460*, 250–253.
18. Tanaka, T.; Jin, H.; Miyata, Y.; Kataura, H. High-Yield Separation of Metallic and Semiconducting Single-Wall Carbon Nanotubes by Agarose Gel Electrophoresis. *Appl. Phys. Express* **2008**, *1*, 114001.
19. Tanaka, T.; Jin, H.; Miyata, Y.; Fujii, S.; Suga, H.; Naitoh, Y.; Minari, T.; Miyadera, T.; Tsukagoshi, K.; Kataura, H. Simple and Scalable Gel-Based Separation of Metallic and Semiconducting Carbon Nanotubes. *Nano Lett.* **2009**, *9*, 1497–1500.
20. Hersam, M. C. Progress towards Monodisperse Single-Walled Carbon Nanotubes. *Nat. Nanotechnol.* **2008**, *3*, 387–394.
21. Britz, D. A.; Khlobystov, A. N. Noncovalent Interactions of Molecules with Single Walled Carbon Nanotubes. *Chem. Soc. Rev.* **2006**, *35*, 637–659.
22. Liu, J.; Hersam, M. C. Recent Developments in Carbon Nanotube Sorting and Selective Growth. *MRS Bull.* **2010**, *35*, 315–321.
23. Wang, H. Dispersing Carbon Nanotubes Using Surfactants. *Curr. Opin. Colloid Interface Sci.* **2009**, *14*, 364–371.
24. Yurekli, K.; Mitchell, C. A.; Krishnamoorti, R. Small-Angle Neutron Scattering from Surfactant-Assisted Aqueous Dispersions of Carbon Nanotubes. *J. Am. Chem. Soc.* **2004**, *126*, 9902–9903.
25. Wallace, E. J.; Sansom, M. S. P. Carbon Nanotube/Detergent Interactions *via* Coarse-Grained Molecular Dynamics. *Nano Lett.* **2007**, *7*, 1923–1928.
26. Nativ-Roth, E.; Shvartzman-Cohen, R.; Bounioux, C.; Florent, M.; Zhang, D.; Szleifer, I.; Yerushalmi-Rozen, R. Physical Adsorption of Block Copolymers to SWNT and MWNT: A Nonwrapping Mechanism. *Macromolecules* **2007**, *40*, 3676–3685.
27. Angelikopoulos, P.; Gromov, A.; Leen, A.; Nerushev, O.;

Bock, H.; Campbell, E. E. B. Dispersing Individual Single-Wall Carbon Nanotubes in Aqueous Surfactant Solutions Below the CMC. *J. Phys. Chem. C* **2010**, *114*, 2–9.
28. Tummala, N. R.; Striolo, A. SDS Surfactants on Carbon Nanotubes: Aggregate Morphology. *ACS Nano* **2009**, *3*, 595–602.
29. Tummala, N. R.; Striolo, A. Curvature Effects on the Adsorption of Aqueous Sodium-Dodecyl-Sulfate Surfactants on Carbonaceous Substrates: Structural Features and Counterion Dynamics. *Phys. Rev. E* **2009**, *80*, 021408-10.
30. Qiao, R.; Ke, P. C. Lipid−Carbon Nanotube Self-Assembly in Aqueous Solution. *J. Am. Chem. Soc.* **2006**, *128*, 13656–13657.
31. Wu, Y.; Hudson, J. S.; Lu, Q.; Moore, J. M.; Mount, A. S.; Rao, A. M.; Alexov, E.; Ke, P. C. Coating Single-Walled Carbon Nanotubes with Phospholipids. *J. Phys. Chem. B* **2006**, *110*, 2475–2478.
32. Calvaresi, M.; Dallavalle, M.; Zerbetto, F. Wrapping Nanotubes with Micelles, Hemimicelles, and Cylindrical Micelles. *Small* **2009**, *5*, 2191–2198.
33. Xu, Z.; Yang, X.; Yang, Z. A Molecular Simulation Probing of Structure and Interaction for Supramolecular Sodium Dodecyl Sulfate/Single-Wall Carbon Nanotube Assemblies. *Nano Lett.* **2010**, *10*, 985–991.
34. Uddin, N. M.; Capaldi, F.; Farouk, B. Molecular Dynamics Simulations of Carbon Nanotube Interactions in Water/Surfactant Systems. *J. Eng. Mater. Technol.* **2010**, *132*, 021012−5.
35. Rastogi, R.; Kaushal, R.; Tripathi, S. K.; Sharma, A. L.; Kaur, I.; Bharadwaj, L. M. Comparative Study of Carbon Nanotube Dispersion Using Surfactants. *J. Colloid Interface Sci.* **2008**, *328*, 421–428.
36. Dong, L.; Joseph, K. L.; Witkowski, C. M.; Craig, M. M. Cytotoxicity of Single-Walled Carbon Nanotubes Suspended in Various Surfactants. *Nanotechnology* **2008**, *19*, 255702.
37. Humphrey, W.; Dalke, A.; Schulten, K. VMD: Visual Molecular Dynamics. *J. Mol. Graphics* **1996**, *14*, 33–38.
38. Grajek, H.; Gryczynski, I.; Bojarski, P.; Gryczynski, Z.; Bharill, S.; Kulak, L. Flavin Mononucleotide Fluorescence Intensity Decay in Concentrated Aqueous Solutions. *Chem. Phys. Lett.* **2007**, *439*, 151–156.
39. Ogunro, O. O.; Wang, X.-Q. Quantum Electronic Stability in Selective Enrichment of Carbon Nanotubes. *Nano Lett.* **2009**, *9*, 1034–1038.
40. Lin, C. S.; Zhang, R. Q.; Niehaus, T. A.; Frauenheim, T. Geometric and Electronic Structures of Carbon Nanotubes Adsorbed with Flavin Adenine Dinucleotide: A Theoretical Study. *J. Phys. Chem. C* **2007**, *111*, 4069–4073.
41. Walther, J. H.; Jaffe, R. L.; Kotsalis, E. M.; Werder, T.; Halicioglu, T.; Koumoutsakos, P. Hydrophobic Hydration of C60 and Carbon Nanotubes in Water. *Carbon* **2004**, *42*, 1185–1194.
42. Li, L.; Bedrov, D.; Smith, G. D. Water-Induced Interactions between Carbon Nanoparticles. *J. Phys. Chem. B* **2006**, *110*, 10509–10513.
43. Pashley, R. M.; Israelachvili, J. N. Molecular Layering of Water in Thin Films between Mica Surfaces and Its Relation to Hydration Forces. *J. Colloid Interface Sci.* **1984**, *101*, 511–523.
44. Besseling, N. A. M. Theory of Hydration Forces between Surfaces. *Langmuir* **1997**, *13*, 2113–2122.
45. Raviv, U.; Klein, J. Fluidity of Bound Hydration Layers. *Science* **2002**, *297*, 1540.
46. Ho, R.; Yuan, J.-Y.; Shao, Z. Hydration Force in the Atomic Force Microscope: A Computational Study. *Biophys. J.* **1998**, *75*, 1076–1083.
47. Patel, N.; Egorov, S. A. Dispersing Nanotubes with Surfactants: A Microscopic Statistical Mechanical Analysis. *J. Am. Chem. Soc.* **2005**, *127*, 14124–14125.
48. Argyris, D.; Cole, D. R.; Striolo, A. Ion-Specific Effects under Confinement: The Role of Interfacial Water. *ACS Nano* **2010**, *4*, 2035–2042.
49. Berendsen, H. J. C.; Grigera, J. R.; Straatsma, T. P. The Missing Term in Effective Pair Potentials. *J. Phys. Chem.* **1987**, *91*, 6269–6271.
50. Wernersson, E.; Jungwirth, P. Effect of Water Polarizability on the Properties of Solutions of Polyvalent Ions: Simulations of Aqueous Sodium Sulfate with Different Force Fields. *J. Chem. Theory Comput.* **2010**, *6*, 3233–3240.
51. Carvalho, E. J. F.; dos Santos, M. C. Role of Surfactants in Carbon Nanotubes Density Gradient Separation. *ACS Nano* **2010**, *4*, 765–770.
52. Cornell, W. D.; Cieplak, P.; Bayly, C. I.; Gould, I. R.; Merz, K. M.; Ferguson, D. M.; Spellmeyer, D. C.; Fox, T.; Caldwell, J. W.; Kollman, P. A. A Second Generation Force Field for the Simulation of Proteins, Nucleic Acids, and Organic Molecules. *J. Am. Chem. Soc.* **1995**, *117*, 5179–5197.
53. Schneider, C.; Sühnel, J. A Molecular Dynamics Simulation of the Flavin Mononucleotide-RNA Aptamer Complex. *Biopolymers* **1999**, *50*, 287–302.
54. Tummala, N. R.; Striolo, A. Role of Counterion Condensation in the Self-Assembly of SDS Surfactants at the Water−Graphite Interface. *J. Phys. Chem. B* **2008**, *112*, 1987–2000.
55. Berendsen, H. J. C.; van der Spoel, D.; van Drunen, R. GROMACS: A Message-Passing Parallel Molecular Dynamics Implementation. *Comput. Phys. Commun.* **1995**, *91*, 43–56.
56. Lindahl, E.; Hess, B.; van der Spoel, D. GROMACS 3.0: A Package for Molecular Simulation and Trajectory Analysis. *J. Mol. Model.* **2001**, *7*, 306–317.
57. van der Spoel, D.; Lindahl, E.; Hess, B.; Groenhof, G.; Mark, A. E.; Berendsen, H. J. C. GROMACS: Fast, Flexible, and Free. *J. Comput. Chem.* **2005**, *26*, 1701–1718.
58. Hess, B.; Kutzner, C.; van Der Spoel, D.; Lindahl, E. GROMACS 4: Algorithms for Highly Efficient, Load-Balanced, and Scalable Molecular Simulation. *J. Chem. Theory Comput.* **2008**, *4*, 435–447.
59. Berendsen, H. J. C.; Postma, J. P. M.; van Gunsteren, W. F.; DiNola, A.; Haak, J. R. Molecular Dynamics with Coupling to an External Bath. *J. Chem. Phys.* **1984**, *81*, 3684–3690.
60. Hoover, W. G. Canonical Dynamics: Equilibrium Phase-Space Distributions. *Phys. Rev. A* **1985**, *31*, 1695.
61. Nosé, S. A Unified Formulation of the Constant Temperature Molecular Dynamics Methods. *J. Chem. Phys.* **1984**, *81*, 511–519.
62. Essmann, U.; Perera, L.; Berkowitz, M. L.; Darden, T.; Lee, H.; Pedersen, L. G. A Smooth Particle Mesh Ewald Method. *J. Chem. Phys.* **1995**, *103*, 8577.
63. Frenkel, D.; Smit, B. *Understanding Molecular Simulations: From Algorithms to Applications*; Academic Press: San Diego, CA, 1996; Vol. 1.
64. Roux, B. The Calculation of the Potential of Mean Force Using Computer Simulations. *Comput. Phys. Commun.* **1995**, *91*, 275–282.
65. Souaille, M.; Roux, B. Extension to the Weighted Histogram Analysis Method: Combining Umbrella Sampling with Free Energy Calculations. *Comput. Phys. Commun.* **2001**, *135*, 40–57.
66. Kumar, S.; Bouzida, D.; Swendsen, R. H.; Kollman, P. A.; Rosenberg, J. M. The Weighted Histogram Analysis Method for Free-Energy Calculations on Biomolecules. I. The Method. *J. Comput. Chem.* **1992**, *13*, 1011–1021.
67. Kumar, S.; Bouzida, D.; Swendsen, R. H.; Kollman, P. A.; Rosenberg, J. M. Multidimensional Free-Energy Calculations Using the Weighted Histogram Analysis Method. *J. Comput. Chem.* **1995**, *16*, 1339–1350.
68. Kumar, S.; Payne, P. W.; Vásquez, M. Method for Free-Energy Calculations Using Iterative Techniques. *J. Comput. Chem.* **1996**, *17*, 1269–1275.